Improvement of Power System Stability with Salp Swarm Algorithm and Fuzzy Type II

Payam Rokni Nakhi[1,5*], Salman Amirkhan[2,5], Javad Safaei Kuchaksaraei[3], Fatemeh Hamedani[4,5]

Abstract –The use of renewable resources in the power system is increasing day by day. Wind energy is one of the forms of renewable energy sources that has been widely available to humans due to the common nature of renewable energy with low concentration (low density). Due to the constant changes of wind and as a result of changes in the power produced by wind farms, uncertainty in the power of the power system will become an integral part. Now, if the permeability of these resources increases, they can directly affect the dynamic stability of the system and the margin of stability of the system will change in power systems expansion, instability was often due to a lack of synchronizing torque. Issues such as the small perturbation stability of local oscillation modes and low-frequency inter-zone oscillation modes became apparent with a significant improvement in power system performance. The paper presents an optimal and coordinated power oscillation damper based on a wind turbine and power system stabilizer (PSS) to maintain the stability of power system and damp inter-area oscillations. The optimal and coordinated design of the PSS located at the generator site and the damper installed in the control section of the doubly-fed induction generator (DFIG) is defined as an optimization problem.

Keywords: Inter-area oscillations, power system stabilizer, doubly-fed induction generator, wide-Area measurement system, dynamic stability, wind farms

Nomenclature

PSS	Power system stabilizer
FACTS	Flexible alternating current transmission system
WAMS	Wide-area measurement systems
WADC	Wide-area damping controller
DFIG	Doubly-fed induction generator
LFO	Low-frequency oscillations
AVR	Automatic voltage regulator

1* Corresponding Author: Department of Power Engineering, Mahdishahr Branch, Islamic Azad University, Mahdishahr, Iran. Email: payamrokni@yahoo.com

2 Department of Electrical Engineering, Aliabad Katoul Branch, Islamic Azad University, Aliabad Katoul, Iran. Email: amirkhan@aliabadiau.ac.ir

3 Department of Power Engineering, SavadkoohBranch, Islamic Azad University, Savadkooh, Iran. Email: dr.safaei@msh-iau.ac.ir

4 Department of Power Engineering, Mahdishahr Branch, Islamic Azad University, Mahdishahr, Iran. Email: Hengamehamedani2020@gmil.com

5 Energy Research Center, Aliabad Katoul Branch, Islamic Azad University, Aliabad Katoul, Iran. Email: amirkhan@aliabadiau.ac.ir

Received: 2012.12.18; Accepted:2022.02.04

FLDC	Fuzzy logic damping controller
$\tau_{d0}^{'}$, $\tau_{q0}^{'}$	d- and q-axis transient time constants
$E_{d}^{'}$, $E_{q}^{'}$	Stator electromagnetic force (EMS) for the transient component of the rotor flux
E_{fd}	Stator EMF for d- and q-axis magnetic field voltage
X_{d} , X_{q}	d- and q-axis synchronous reactance
$X_{d}^{'}$, $X_{q}^{'}$	d- and q-axis transient reactance of
I_{d} , I_{q}	d- and q-axis current of the stator
Pe	The synchronous generator electrical power output
D	Damping factor

1. Introduction

The ability of a power system to maintain synchronous state after a perturbation when the system returns to its original state or a new operating point is called stability [1]. This definition is generally applicable to the entire power system and can be used to study the stability of a particular generator or a large number of generators, or to evaluate stability for changes in one-point load or load in a particular region. Objective when examining the stability of a system, the most important objective is to study its characteristics during turbulence. Because the power system is a nonlinear system that is constantly faced with disturbances such as changes in load and output, the system must be able to adapt to new conditions. These disturbances are small, but severe examples, such as short-circuit faults, can change the structure of the system ([2],[3]).These dynamic instabilities caused by the imbalance between mechanical input power and electrical output power and lack of damping torque will lead to local and inter-area oscillations in the power system [4]. These oscillations frequency is in the range of 0.2-2 Hz. Local oscillations refers to oscillations that depend on a single generator or a single power plant in the frequency range of 0.8-2 Hz. Inter-area oscillations with a frequency range of 0.2-0.8 Hz appear when generators in one area oscillate against generators in the other area. Inter-area oscillations further threaten the stability of the power system due to their low attenuation [5]. One of the types of variable speed turbines is wind turbines equipped with dual feed induction generator (DFIG). Most wind turbines today are equipped with induction generators from both sides. In this type, the induction generator of the winding rotor is connected to the power grid through the stator and the rotor is connected to the power grid via the ac / dc / ac variable frequency (VFC) electronic power converter with a rated power of about 25-30% of the nominal generator to the power grid. Connects. The electronic power converter consists of a rotor side converter (RSC) and a grid side converter (GSC) which are connected back to back via a dc capacitor. The main drawback of variable speed wind turbines, especially turbines equipped with DFIG, is their performance during a short circuit in the network. Short circuit on the power system, even if it is far from the location of the wind turbine, causes a voltage drop at the connection point of the wind turbine to the power grid. The effect of the presence of wind resources in the design and coordination of power system stabilizers should be carefully studied ([6]-[8]). Dynamic stability is one of the most important issues in the field of power system studies that has attracted the attention of power engineers in recent decades. The problem starts with the fact that the voltage and frequency of the power system must be within an acceptable value in the event of disturbances such as load changes, loss of output or line failure [9].

2. Excitation system modeling

The excitation system model, used in this paper, is the standard IEEE AC4A model. Fig. 2 illustrates the block diagram of the excitation system [10].

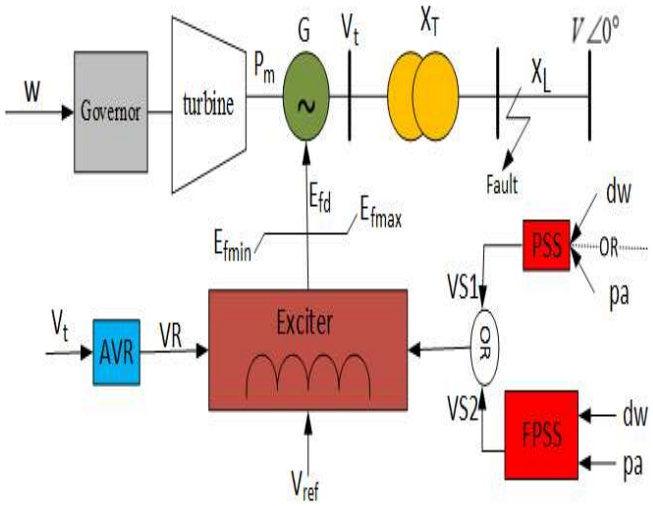

Fig. 1. The excitation system block diagram [10]

The dynamic equations of the excitation system are obtained as follows:

$$\dot{E}_{fdi} = \frac{K_{Ai}}{T_{Ai}} X_{E2i} - \frac{1}{T_{Ai}} E_{fdi} \quad (1)$$

$$\dot{X}_{E1i} = \frac{1}{T_{Ri}} V_{Ti} - \frac{1}{T_{Ri}} X_{E1i} \quad (2)$$

$$\dot{X}_{E2i} = \frac{1}{T_{Bi}}\left(\frac{T_{Ci}}{T_{Ri}} - 1\right) X_{E1i} - \frac{1}{T_{Bi}} X_{E2i} + \frac{T_{Ci}}{T_{Bi}T_{Ri}} V_{Ti} + \frac{1}{T_{Bi}} V_{refi} \quad (3)$$

Where V_{Ti} denotes the terminal voltage of the synchronous generator, V_{refi} is the reference voltage, K_{Ai} is the amplitude, and T_{Ai} represents the time constant of the excitation system. The excitation system is a direct current (DC) source for the synchronous machine field winding, which controls the current and voltage of the excitation winding field.

2.1 PSS modeling

The PSS complementary signal to the excitation and auxiliary control systems of DFIG-based wind farms will be able to optimally enhance the system dynamic stability. The PSS modulates the generator excitation to create a damping electrical torque component to dampen the oscillations. This method is very important because its implementation cost is lower than other methods [11].

The block diagram of the damper, considered in this paper, is given in Fig. 3 [12]. In this model, a damper with complex zeros is included in the compensator model [13]. The first block is the lag-lead compensator, whose zeros and poles can be optimally tuned. This block provides a suitable lead characteristic for lag compensation between the exciter input and the electric torque of the generator (air gap). The second block for the high-pass filter or washout filter removes the steady-state effect with a time constant of TW, which allows the input signal corresponding to the speed changes to pass without variations in the steady-state [14].

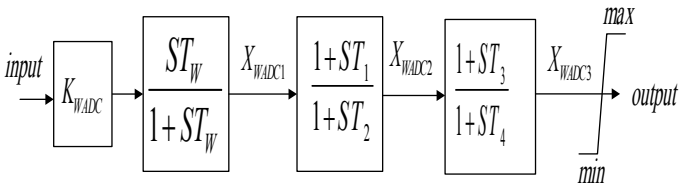

Fig. 2. The PSS block diagram [25]

The dynamic equations of the PSS according to the block diagram of Fig. 3 are obtained as follows:

$$\dot{X}_{WADC1} = -\frac{1}{T_W} X_{WADC1} + K_{WADC} \frac{1}{120\pi} \dot{\omega}_{ij} \quad (4)$$

$$\dot{X}_{WADC2} = -\frac{1}{T_2} X_{WADC2} + \frac{1}{T_2} X_{WADC1} + \frac{T_1}{T_2} \dot{X}_{WADC1} \quad (5)$$

$$\dot{X}_{WADC3} = \frac{1}{T_4} X_{WADC2} + \frac{1}{T_4} X_{WADC1} + \frac{T_3}{T_4} \dot{X}_{WADC2} \quad (6)$$

Where T4… T1 > 0 are stabilizing parameters that must be optimally adjusted and KWADC denotes the gain of the WADC, which can have a constant and optimal value.

2.2 DFIG modeling

The wind turbine is connected to the DFIG by a mechanical system. The mechanical system consists of one low-speed and one high-speed shaft which are separated by a gearbox. The wound-rotor induction generator in this structure feeds both the rotor and the stator of the electrical network. In this machine, the stator is directly connected to the mains; however, the rotor is in connection with the mains by a frequency-variable AC/DC/AC power electronics converter. To generate power at a constant frequency and voltage for an electrical network in the speed range between sub-synchronous and super-synchronous speeds, it is essential to control the transmission power between the rotor and the mains both in terms of quantity and direction.

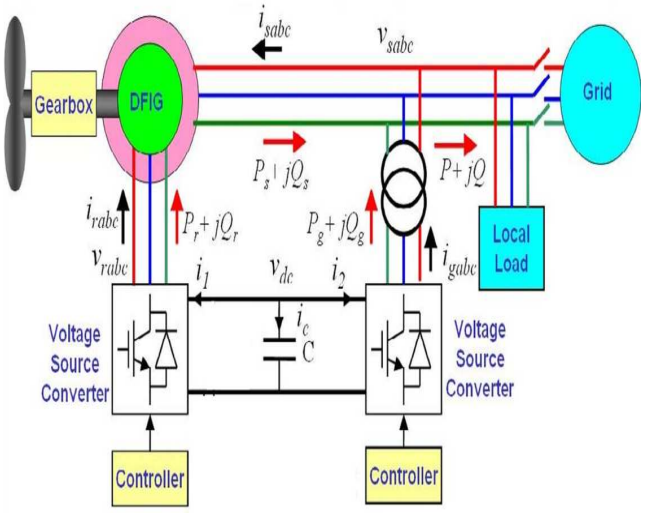

Fig. 3. Structure of the DFIG

Wind turbine control focuses on optimizing the wind turbine output power by controlling the blade angle as well as avoiding excessive power of strong winds. The DFIG control system is composed of RSC and GSC controllers to control its active and reactive power. Fig. 5 depicts the block diagram of the RSC controller. The q- and d-axis loops are used to adjust the active power (P) of the DFIG and the reactive power of the DFIG (Q) stator, respectively. Active and reactive power is adjusted using a classic proportional-integral (PI) control. The GSC control loop, shown in Fig. 6, serves two purposes: 1) to regulate the DC-bus voltage for the DFIG by passing active power through GSC and RSC, and 2) to adjust the reactive power of the DFIG GSC (Qg). Similar to the RSC, the classic PI controller is used in both the DC voltage control loop and the Qg controller. Due to the presence of two separate controllers in the RSC, additional functions can be performed by complementary auxiliary control (CAC). If the CAC is added to the active power or reactive power control loop, active or reactive power modulation will be obtained [15].

The three-phase DFIG dynamic equation in the d-q synchronous rotating reference frame is expressed as follows [16]:

$$V_{ds} = V_s I_{ds} - \omega\lambda_{qs} + \frac{d\lambda_{ds}}{dt} \quad (7)$$

$$V_{qs} = V_s I_{qs} + \omega\lambda_{ds} + \frac{d\lambda_{qs}}{dt} \quad (8)$$

$$V_{dr} = V_s I_{dr} - s\omega\lambda_{qr} + \frac{d\lambda_{dr}}{dt} \quad (9)$$

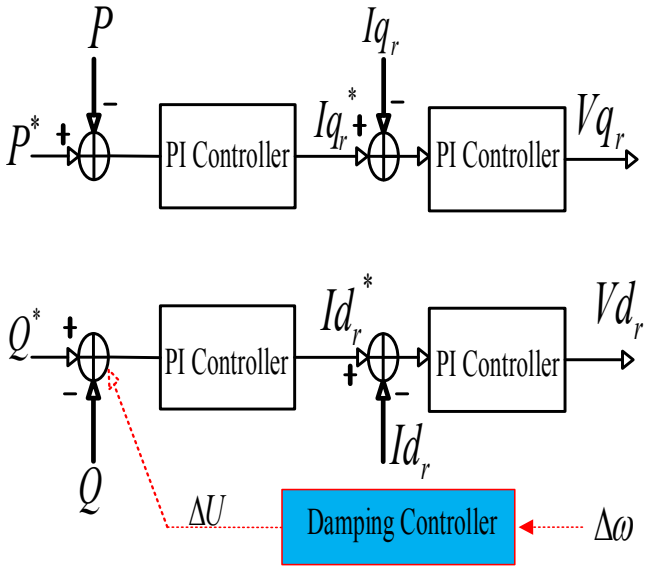

Fig. 4. The DFIG RSC control structure [15]

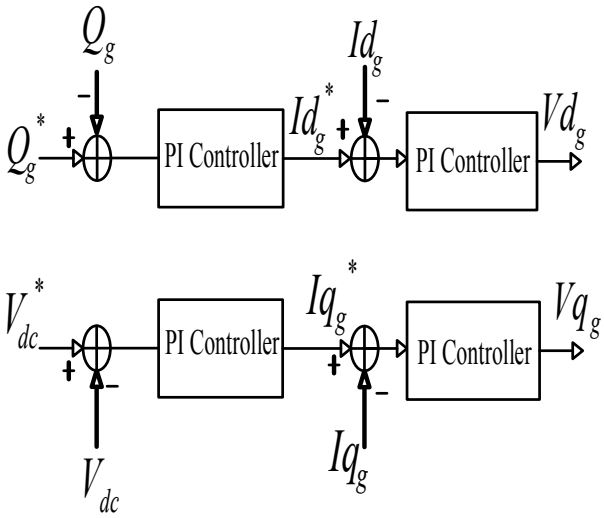

Fig. 5. The DFIG GSC control structure [15]

Where, ω_s serves as the reference frame synchronous rotational speed and $s\omega_s = \omega_s - \omega_r$ denotes the slip frequency. The DFIG flux linkage is given by the following equations:

$$\lambda_{ds} = L_{ls} i_{ds} + L_m(i_{ds} - i_{dr}) = L_s i_{ds} + L_m i_{dr} \quad (10)$$

$$\lambda_{qs} = L_{ls} i_{qs} + L_m(i_{qs} + i_{qr}) = L_s i_{qs} + L_m i_{qr} \quad (11)$$

$$\lambda_{dr} = L_{lr} i_{dr} + L_m(\mathrm{i}_{ds} + \mathrm{i}_{dr}) = \mathrm{L}_m i_{ds} + L_r i_{dr} \quad (12)$$

$$\lambda_{qr} = L_{lr} i_{qr} + L_m(\mathrm{i}_{qs} + \mathrm{i}_{qr}) = \mathrm{L}_m i_{qs} + L_r i_{qr} \quad (13)$$

In the above equations, $L_s = L_m + L_{ls}$, $L_r = L_m + L_{lr}$, L_{ls}, L_m, and L_{lr} show the stator and rotor linkage inductances and the mutual inductance. DFIG electromagnetic torque is expressed as follows:

$$T_e = \frac{3}{2}\frac{p}{2} L_m(\mathrm{i}_{qs}\,\mathrm{i}_{dr} - \mathrm{i}_{ds}\,\mathrm{i}_{qr}) \quad (14)$$

P indicates the number of poles of the induction machine. By ignoring the power losses related to the stator resistance, the stator active and reactive powers are obtained as the following equations:

$$P_s = \frac{3}{2}(\mathrm{V}_{ds}\,\mathrm{i}_{ds} + \mathrm{V}_{qs}\,\mathrm{i}_{qs}) \quad (15)$$

$$Q_s = \frac{3}{2}(\mathrm{V}_{qs}\,\mathrm{i}_{ds} - \mathrm{V}_{ds}\,\mathrm{i}_{qs}) \quad (16)$$

And the active and reactive power of the rotor is determined by:

$$P_r = \frac{3}{2}(\mathrm{V}_{dr}\,\mathrm{i}_{dr} + \mathrm{V}_{qr}\,\mathrm{i}_{qr}) \quad (17)$$

$$Q_r = \frac{3}{2}(\mathrm{V}_{qr}\,\mathrm{i}_{dr} - \mathrm{V}_{dr}\,\mathrm{i}_{qr}) \quad (18)$$

In the d-q reference frame, there are mathematical relationships between the d- and q-axis components:

$$i_{qs} = \frac{-L_m i_{qr}}{L_s} \quad (19)$$

$$i_{ds} = \frac{L_m(\mathrm{i}_{ms} - \mathrm{i}_{dr})}{L_s} \quad (20)$$

$$T_e = \frac{-\frac{3}{2}\frac{p}{2} L_m{}^2 i_{ms} i_{qr}}{L_s} \quad (21)$$

$$Q_s = \frac{3}{2}\omega_s L_m{}^2 i_{ms}(\mathrm{i}_{ms} - \mathrm{i}_{dr})\,\mathrm{L}_s \quad (22)$$

Where

$$V_{dr} = r_r i_{dr} + \sigma L_r \frac{di_{dr}}{dt} - s\omega_s \sigma L_r i_{qr} \quad (23)$$

$$V_{qr} = r_r i_{qr} + \sigma L_r \frac{di_{qr}}{dt} - s\omega_s(\sigma L_r i_{dr} + \frac{L_m{}^2 i_{ms}}{L_s}) \quad (24)$$

$$i_{ms} = \frac{V_{qs} - r_s i_{qs}}{\omega_s L_m} \quad (25)$$

$$\sigma = 1 - \frac{L_m{}^2}{L_s L_r} \quad (26)$$

The above equations show that the DFIG rotor (ω_r) speed can be controlled as a result of the stator active power by adjusting the q-axis (I_{qr}) current component. Also, according to Eq. (16), the stator reactive power is controlled Qs by adjusting the d-axis component of the rotor current (I_{dr}). Consequently, the I_{qr} and I_{dr} reference values are directly obtained through adjusting the DFIG stator reactive power, its rotor speed or stator power.

3. Uncertainty Modeling

Concerning the intermittent nature of wind with long-term measurements at different time intervals, the probability density function (PDF) of wind speed is used to calculate energy [18]. Weibull distribution is one of the continuous probabilistic distributions. Although it was first introduced by Freche, a French scientist, in 1927 and then used by Resin and Ramler in 1933 to describe the particle size distribution, it is named after Valdi Weibull, who described it in details in 1951. Various statistical methods have been employed to determine the wind energy potential in the desired location and to estimate its output energy. In most cases, the Weibull statistical model provides a very suitable correlation with wind speed distribution. Power output by wind turbines varies over time depending on wind speed. The wind turbine output power approximate relationship is as follows: wind power generation depends on wind speed and wind turbine blade engagement. Turbine output power can take one of the three values given below [19]:

$$P_{GWT}(v) = \begin{cases} 0 & 0 \le v \le v_a \,..\sigma..\, v \ge v_\omega \\ P_{rWT}\dfrac{V - V_a}{V_r - V_a} & v_a < v < v_r \\ P_{rWT} & v_r < v < v_\omega \end{cases} \quad (27)$$

In this equation, P_{wt} is the turbine mechanical output power (W), ρ is the air density (kg/m3), A_{wt} is the turbine displacement range (m_2), V is the wind speed (m/s), C_p is the turbine performance coefficient (or power factor) and Vcutin, Vrated, and Vcutout denote the turbine cut-in, rated, and cut-off speed (m/s). PDFs were used to describe the

wind speed random behavior. Wind speeds over a predetermined time were estimated using Weibull PDF:[16]

$$f(V) = \frac{k}{c}\left(\frac{v}{c}\right)^{k-1} \exp\left(-\left(\frac{v}{c}\right)^{k}\right) \quad (28)$$

$$k = \left(\frac{\sigma}{\mu}\right)^{-1.086} \quad (29)$$

$$c = \frac{\mu}{\Gamma(1+\mathrm{k}^{-1})} \quad (30)$$

4. Inter-area oscillation damper design

An optimization problem-solving method has been applied for designing the PSS in this study. To solve the given optimization problem, several objective functions are considered. These objective functions are limited by constraints. The objective functions, constraints, and properties of objective functions used for designing the PSS are given in the following subsections. Besides, the implementation of the SSA, used for designing the PSS, is described.

4.1. Salp swarm algorithm

The Salp swarm algorithm (SSA), inspired by the social behavior of Salps, was first proposed by Mirjalili et al. [20] in 2017. Salps are classified as a species of a family of Salpidae, which have a clear, tube-shaped body. Their body tissue is very similar to that of jelly fish and they move very much like jelly fish, in that water is pumped through their body to provide forward thrust. The salp shape either individually or in groups is shown in Fig. 6.[16]

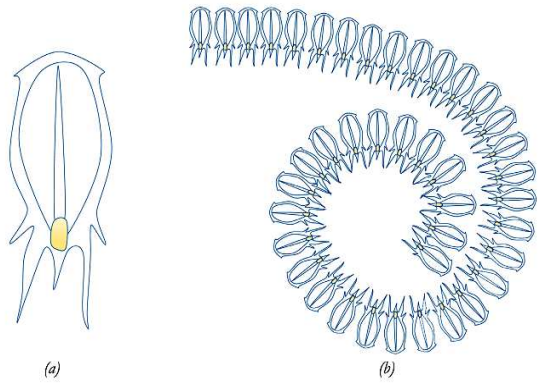

Fig. 6. (a) Single salp, (b) a group of salps (chain of salp)

In modeling the SSA, their social and chain behavior has been used for better movement using fast coordinated changes and foraging behavior. To mathematically model salp chains, the population is first allottedinto two groups: leader and followers. The group leader is a salp in front of the chain, and the other salps are considered followers. As the name suggests, the leader guidesthe group, and the followers follow each other (and directly or indirectly follow the leader). Like other swarm-based methods, the salps position is defined in an n-dimensional search space in which n is the variables number of a given problem. Therefore, all salps position is stored in a two-dimensional matrix, x. It is also assumed that there is a food source called F in the search space as the group objective. The following equation updates the leader's position:

$$x_j^1 = \begin{cases} F_j + c_1 \times ((ub_j - lb_j) \times c_2 + lb_j) & c_3 \geq 0 \\ F_j - c_1 \times ((ub_j - lb_j) \times c_2 + lb_j) & c_3 < 0 \end{cases} \quad (31)$$

where x_j^1 indicates the first salp (leader) position in the j^{th} dimension, Fj represents the food source position in the j^{th} dimension, ub_j shows the upper boundary of the j^{th} dimension, lbj is the lower boundary of the j^{th} dimension, c_1, c_2, and c_3 are random numbers. Equation (2) shows that the leader updates its position only concerning the food source. The coefficient c1 is the most important parameter in the SSA because it balances the exploration and exploitation phases as follows:

$$c_1 = 2e^{-(\frac{4l}{L})^2} \quad (32)$$

Where l is the current iteration and L represents the iterations maximum number. Parameters c_2 and c_3 are random numbers being uniformly generated at the range [0, 1]. These indicate if the next position in the j^{th} dimension should be infinitely positive or infinitely negative, and also determine the step size. The following equations are used to update the position of the followers (Newton's law of motion):

$$x_j^i = \frac{1}{2} a \times t + v_0 \times t \quad (33)$$

Where $i \geq 2$, x_j^1 indicates the ith follower position in the jth dimension, it is time, v0 denotes the initial velocity, $a = \frac{v_{final}}{v_0}$ and $v = \frac{x - x_0}{t}$ in which . Since the time in optimization is the same as the iteration, the difference between the iterations is 1, and considering $v_0 = 0$, this equation can be rewritten as follows:

$$x_j^i = \frac{1}{2}(x_j^i + x_j^{i-1}) \quad (34)$$

where $i \geq 2$, x_j^i shows the ith follower salp position in the jth dimension. Using Eqs. (5) and (8), salp chains can be simulated. The SSA pseudocode is given in Fig. 7 [41].

the first salps population initialization and generation of concerning the upper and lower boundaries, *ub* and *lb*

While (until the termination criteria are satisfied)

Calculate objective function for each agent

Select the best search agent

Update c_1 using Eq. (17)

For each salp

If (i==1)

Update the leader salp position using Eq. (18)

Otherwise

Update the follower salps positions using Eq. (20)

End if

End for

Check if the salps are in the range between *lb* and *ub*

End

Fig. 7. Pseudocode of the SSA

4.2.Objective functions and constraints

Inter-area oscillations are related to speed changes and speed differences between generators in different areas. The oscillations amplitude caused by speed differences between generators is low when low-frequency oscillations are much more damped. To do this, , the system stability can be improved by minimizing the integral below the surface of these signals as an objective function. The objective function used in this study is given in Eq. (35) [25].

$$J = \int_0^{t_{sim}} t.\Delta\omega_{ij}^2.dt \quad (35)$$

Where, $\Delta\omega_{ij}$ is the speed difference between generators i and j in different areas. To do so, the optimization problem with constraints is expressed as Eq. (36) [16]:

$$\begin{aligned} &Minimize\ J \\ &Subject\ to: \\ &T_1^{\min} \leq T_1 \leq T_1^{\max} \\ &T_2^{\min} \leq T_2 \leq T_2^{\max} \\ &T_3^{\min} \leq T_3 \leq T_3^{\max} \\ &T_4^{\min} \leq T_4 \leq T_4^{\max} \\ &K_{WADC}^{\min} \leq K_{WADC} \leq K_{WADC}^{\max} \\ &K_1^{\min} \leq K_1 \leq K_1^{\max} \\ &K_2^{\min} \leq K_2 \leq K_2^{\max} \end{aligned} \quad (36)$$

5. Simulation results

This section addresses simulations and the simulation results presentation obtained from the proposed method on the system under study.

5.1 The system under study

Since the present study aims to damp inter-area oscillations and use and analyze the effect of the DFIG-based damper, the IEEE multi-machine power system is employed to investigate the proposed method. The system under study is a multi-machine three-area system [23]. The system under study consists of three areas. The system consists of four 900 mV generators located in two areas, which are connected to each other through two 220 km communication lines. This system is an extended case of the standard four-machine Condor system. The nonlinear simulation results of the system for unstable conditions are shown by applying a three-phase fault in Bus 8 for 200 ms. In this case, the system is open-loop and no dampers and PSSs are connected to the generators or the DFIG. The power system becomes unstable in the absence of a stabilizer

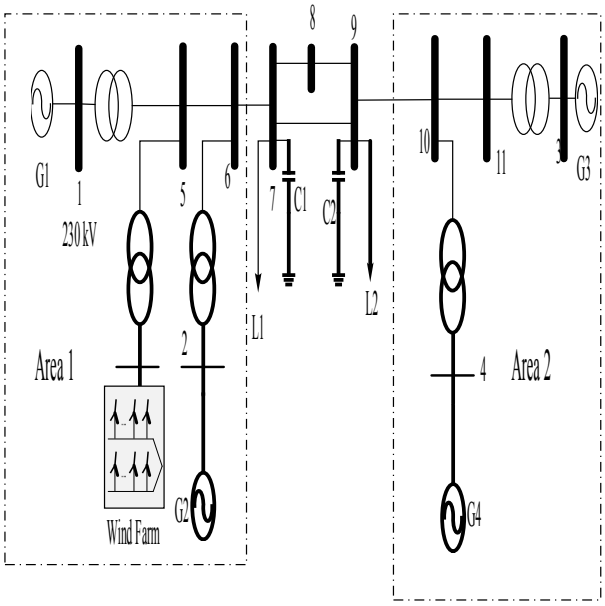

Fig. 8. The six-machine system with a DFIG

In this case, the speed difference between the generators of different areas increases, and generators lose synchronism, and thus, the whole system loses its synchronization. Fig. 9 depicts the generators speed differences of different areas, which represent the inter-area oscillations, along with the transmission power oscillations between the areas. According to the simulation results obtained for the six-machine three-area system in the absence of stabilization, it can be said that the system is unable to maintain stability after applying the fault; thus, after a while, it steps out of synchronism mode and becomes completely unstable.

To stabilize the power system, the proposed method in this paper has been used, which has been studied in two scenarios.

Scenario 1: At rated load, the wind speed is 12 meters per second

Scenario 2: In case of 20% system overload, the wind speed is 12 meters per second and one of the communication lines is cut off.

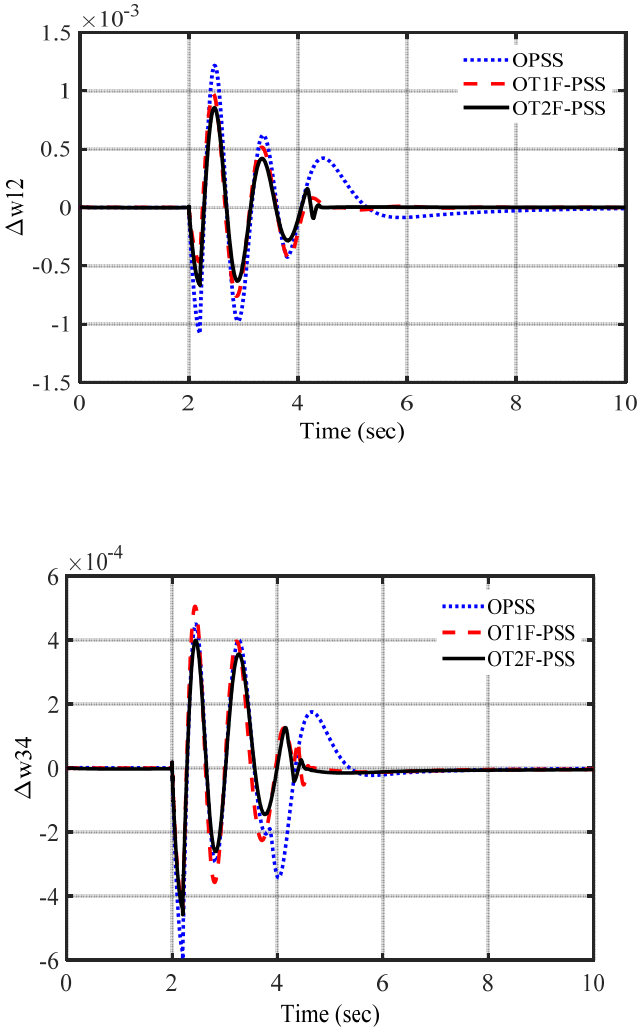

Fig. 9. The system simulation results under study in the open-loop mode in the absence of a damper

5.1.1 Scenario 1

In this case, low-frequency oscillations are suitably damped using wind turbines and the PSS connected to the generator. Fig. 11 shows the generators speed difference in different areas of the power system and the transmission power between different areas. Fig. 11 demonstrates the active and reactive power generated by the wind turbine. According to the simulation results, one can conclude that the presence of DFIG-based wind turbines equipped with WADC improves the system stability and increases the inter-area oscillations damping.

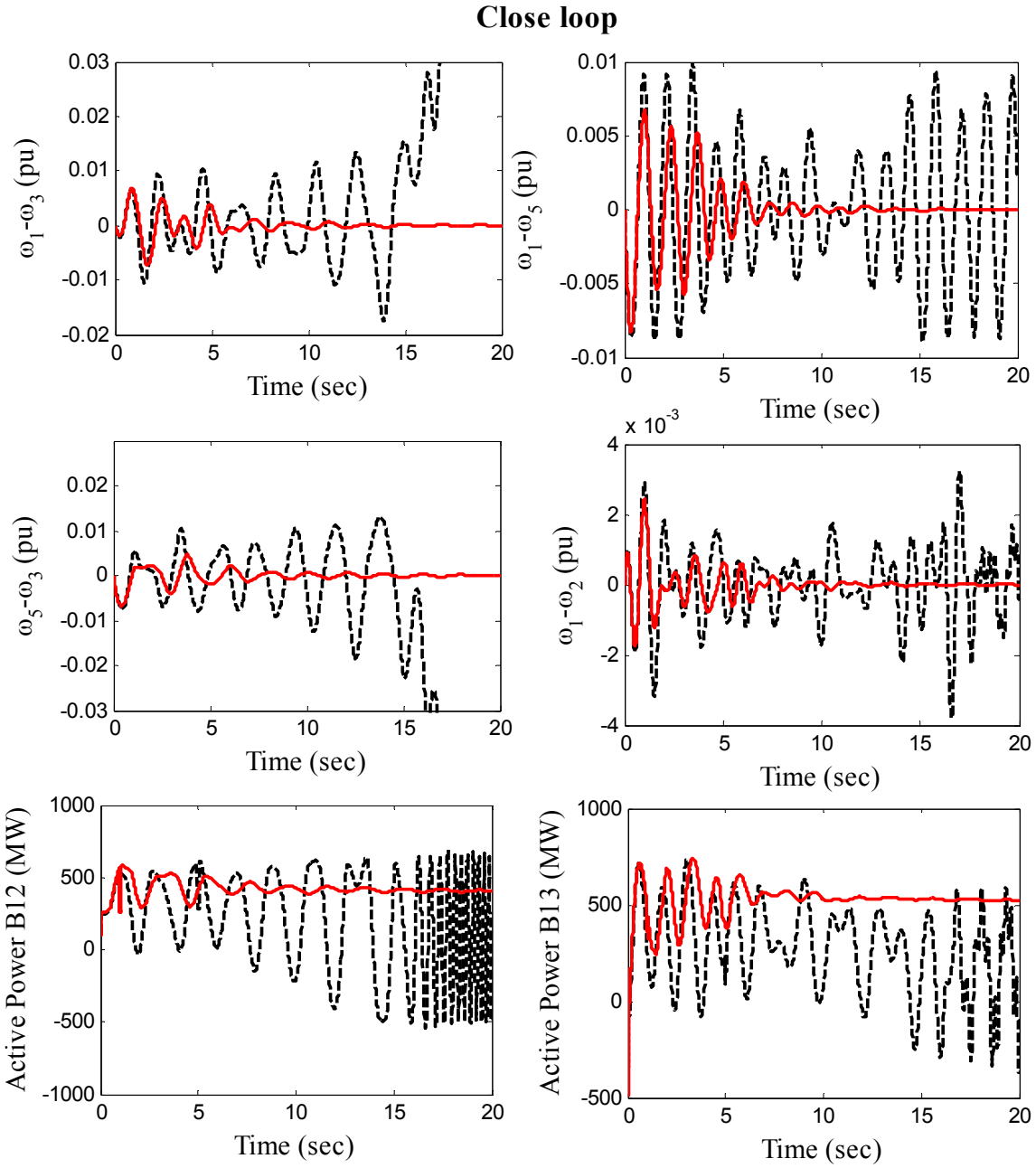

Fig. 10. The system simulation results under study in the closed-loop mode and the DFIG presence (-- open-loop, - closed-loop)

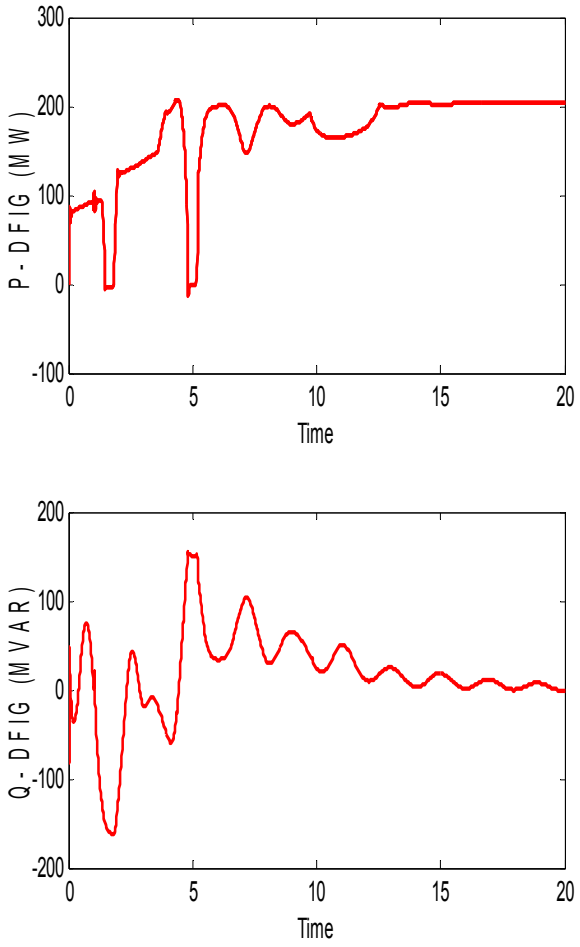

Fig. 11. The DFIG-based wind turbine active and reactive power

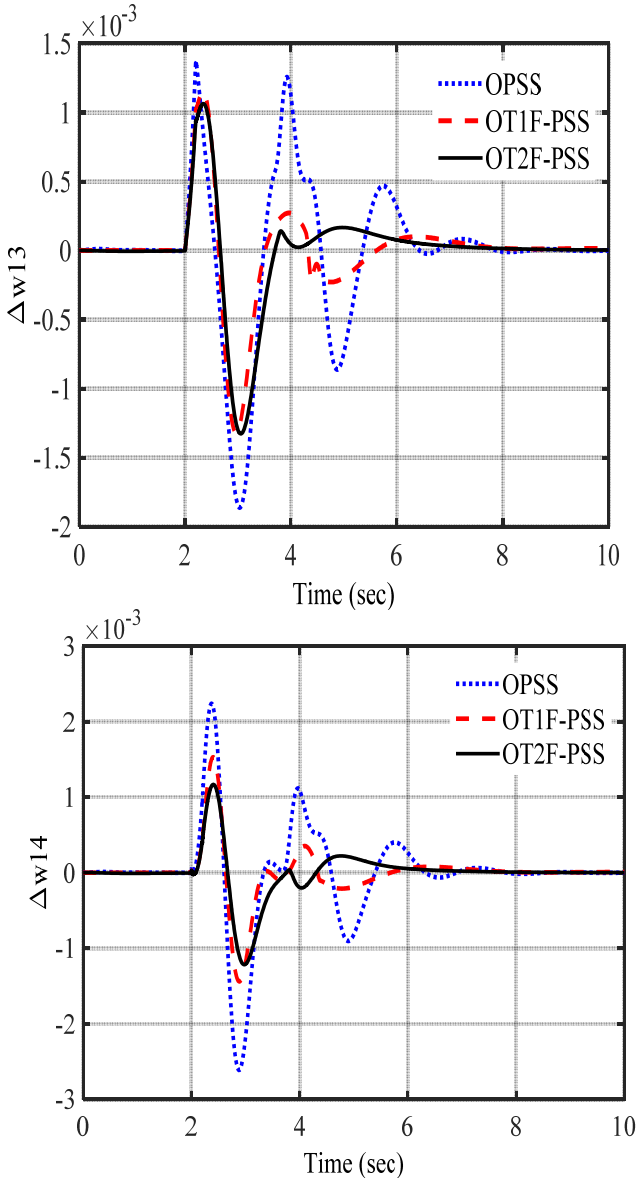

Fig. 12.load20% increase and wind speed is 12 m/s; and the transmission line between bus 7 and 9 is disconnected

5.1.2 Scenario 2:

In case of 20% system overload, the wind speed is 12 meters per second and one of the communication lines is cut off.

In this section, to evaluate the robustness of the WADC, designed using the proposed method, which is installed on the DFIG control loop, the simulation results are provided for different time delays and the results are analyzed. The nonlinear simulation results of the three-area system for different time delays are shown in Fig. 12. The wind speed is also randomly determined through the Weibull PDF. According to the simulation results, for different time delays applied to WADC, the stability of the system has not reduced or become unstable with increasing time delay, and DFIG continues to dampen low-frequency oscillations.

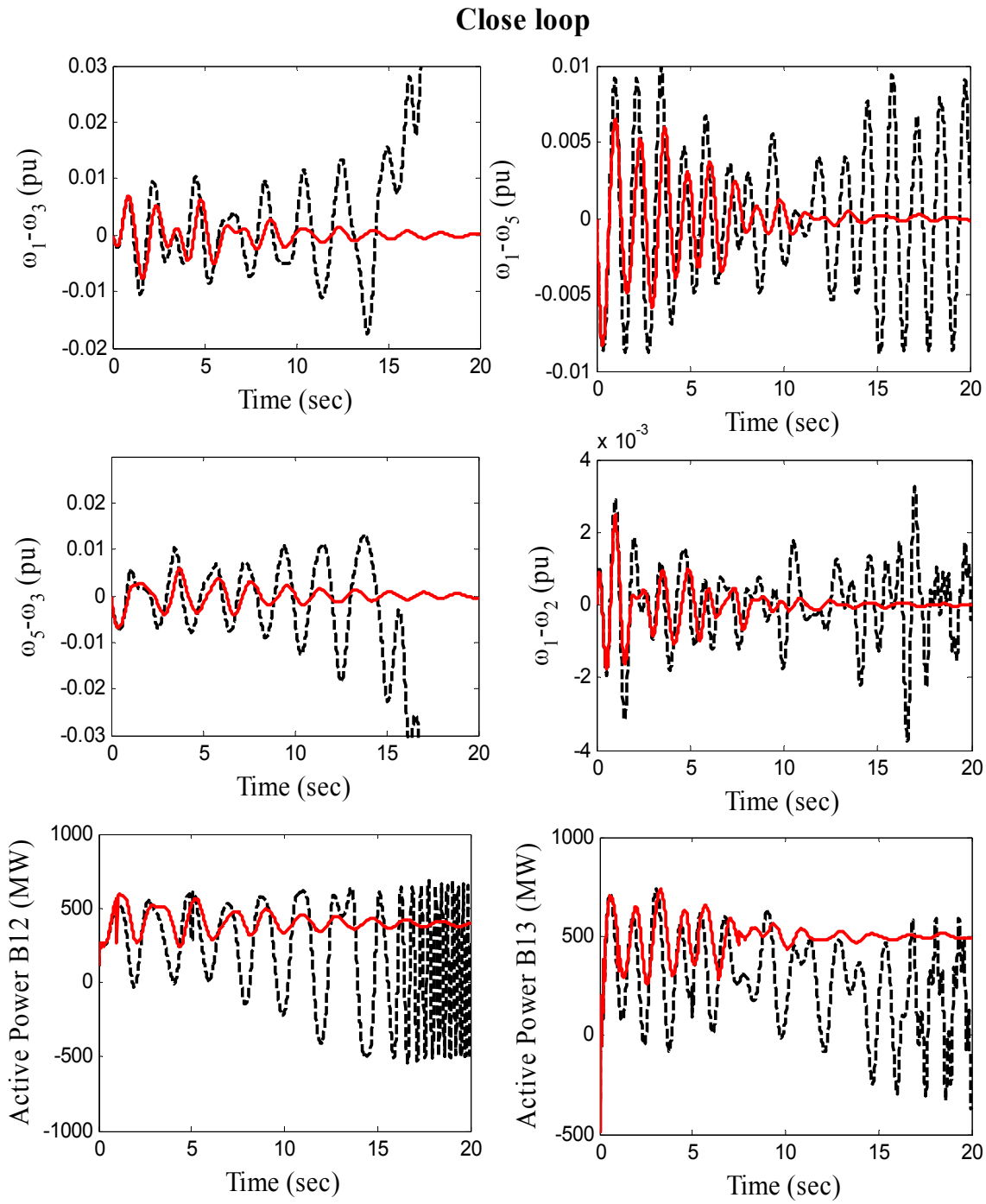

Fig. 13. The system simulation under study in the closed-loop mode in the presence of the DFIG and considering wind speed uncertainty and time delay (- - open-loop, - closed-loop)

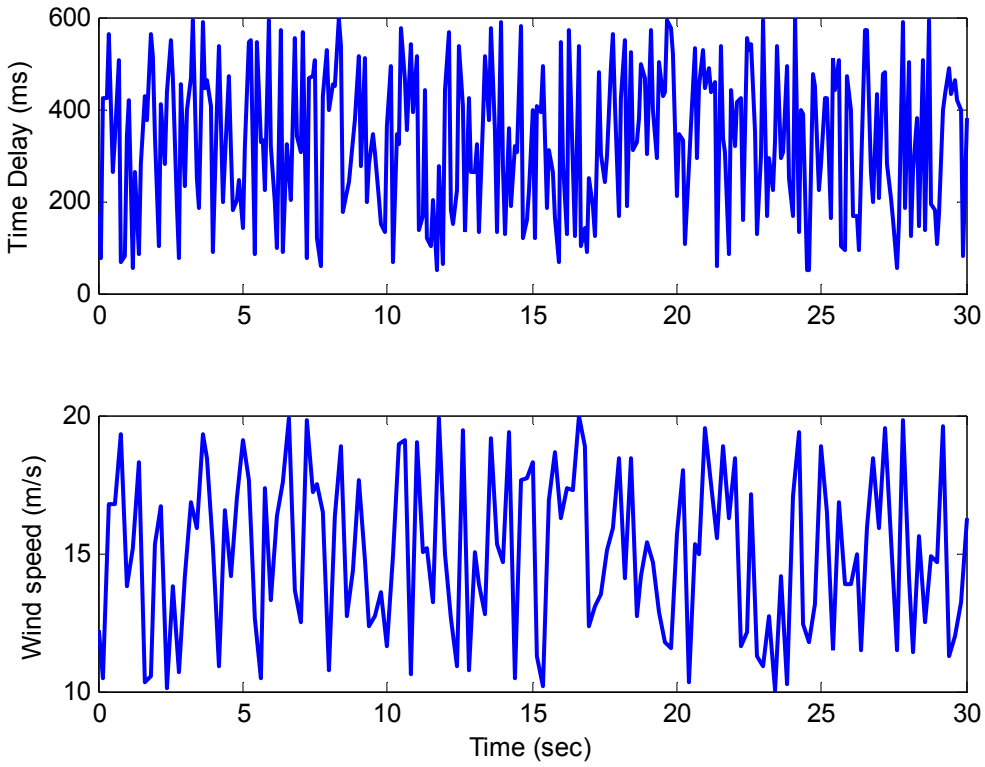

Fig. 14. Random changes in time delay and wind speed

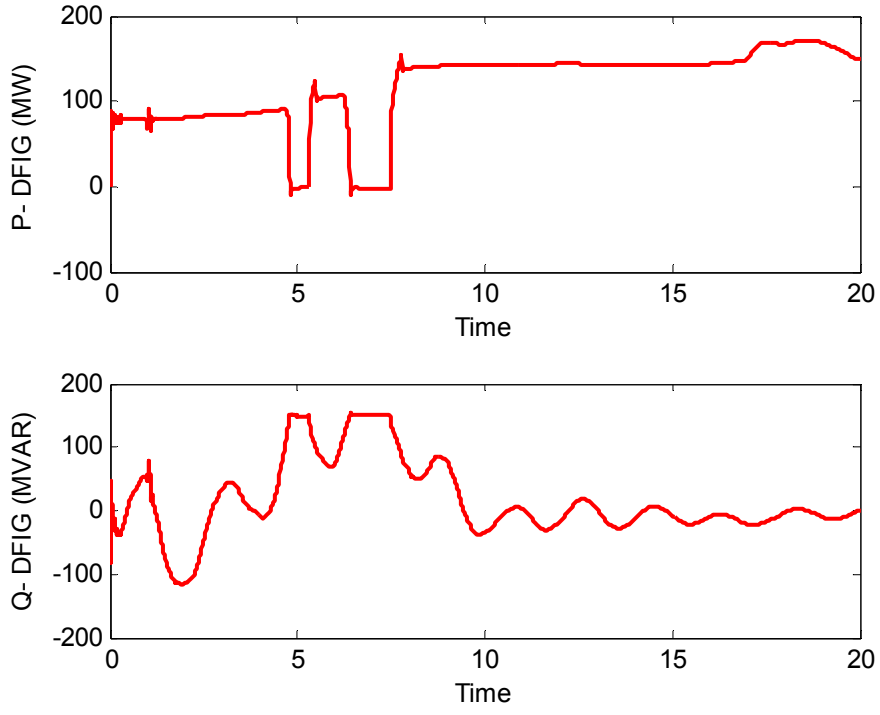

Fig. 15. The DFIG-based wind turbine active and reactive power

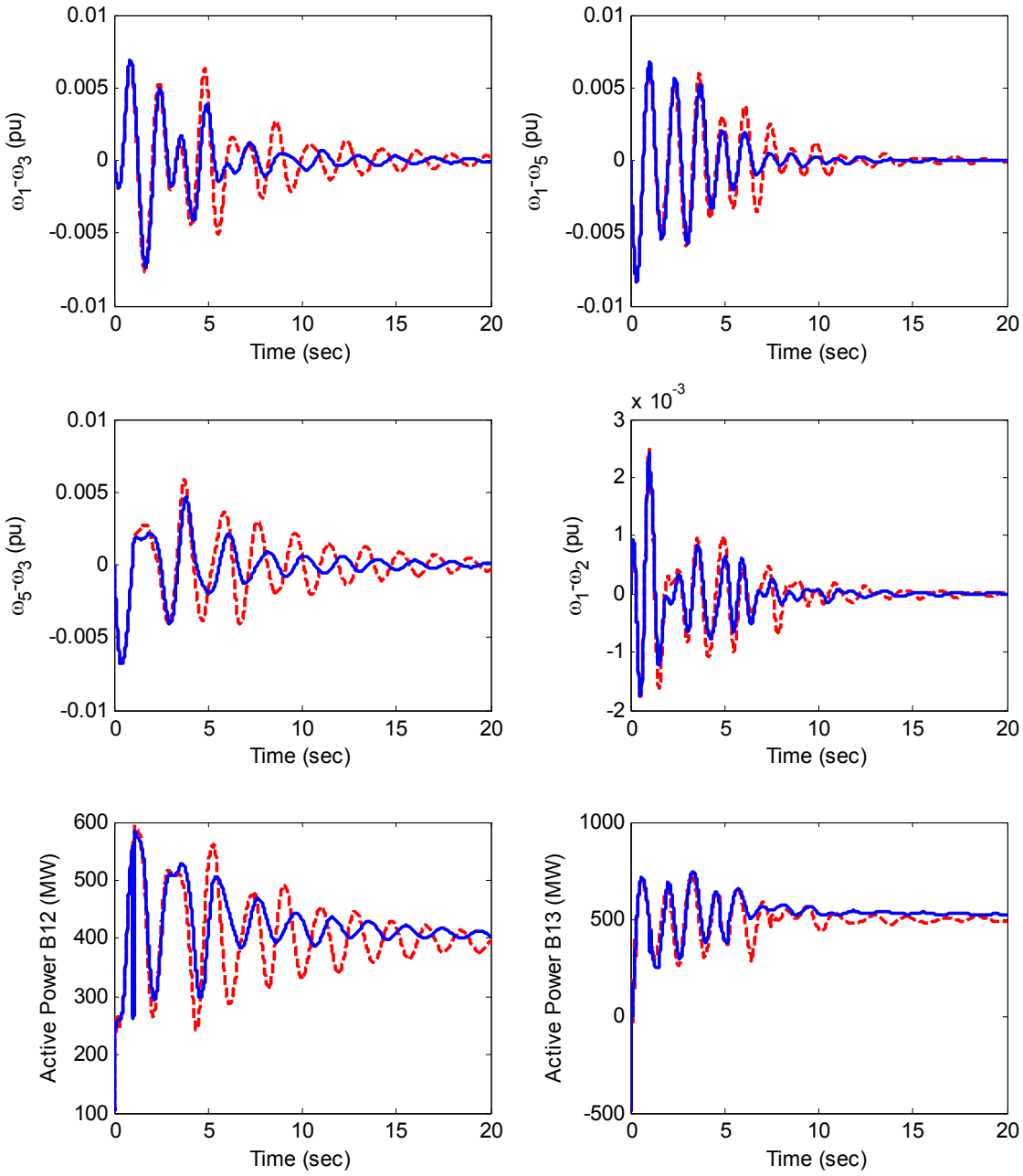

Fig. 16. The system simulation under study in the closed-loop mode in the presence of the DFIG and considering wind speed uncertainty and time delay (- - with time delay, - without time delay)

5.2 Numerical comparison

To analyze power systems in the time domain, various tools are expressed that are a function of system error and their damping time. Depending on the type of study performed, any of these criteria can be used. The most important indices are the absolute value integral of the error function (IAE), the square integral of the error function (ISE), the time integral of the absolute value of the error function (ITAE), and finally the square integral of time in the square of the error function (ISTSE). . The relationships of these indicators are given below.To evaluate and compare the scenarios presented in the previous sections, this section uses different evaluation indices such as ISE, ITEA, and ITSE for different signals in the case of zero time delay. In the above relations, $e(t)$ and t represent the system error and damping time, respectively. Equations (37)-(39) show how to calculate these evaluation indices:

$$ISE = \int_0^{t_{sim}} \Delta\omega_{ij}^2 .dt \tag{37}$$

$$ITEA = \int_0^{t_{sim}} t.|\Delta\omega_{ij}|dt \tag{38}$$

$$ITSE = \int_0^{t_{sim}} t.\Delta\omega_{ij}^2 .dt \tag{39}$$

Table 1. The evaluation index of the three-area power system

	Signal	ISE	ITEA	ITSE
No Device	$\Delta\omega_{13}$	11.8486	185.964	253.5451
	$\Delta\omega_{15}$	0.039874	8.1698	0.13547
	$\Delta\omega_{35}$	12.6589	191.3547	256.3695
DFIG	$\Delta\omega_{13}$	0.011125	2.2549	0.01985
	$\Delta\omega_{15}$	0.016548	4.1254	0.019684
	$\Delta\omega_{35}$	0.008659	2.6987	0.015489

6. Conclusion

At the beginning of the article, an overview of stabilizers and different types of power system stabilizers and then the methods used to design the stabilizer were reviewed. In the first part, the design of stabilizers and their methods have been analyzed and studied in the absence of uncertainty about power systems, and in the second part, studies have been performed in the presence of uncertainty. Uncertainty in system load is one of the most important causes of uncertainty. Evaluations indicate that uncertainties should be considered in small signal stability studies of the power system, and regardless of them will cause the results to be invalid and the designs to be incorrect. And so we went to fuzzy logic of the second type and the uncertainties in power systems were studied. Although many studies and studies have been done in the field of designing various types of stabilizers of a power system, but in most cases, the uncertainties in the power system have not been investigated. In the presence of uncertainties in the power system that are not considered in the designs, the controllers may not be able to respond properly and may reduce the margin of stability in the power system. Many control designs are based on the system model, the relationship between the models and the actual performance of the system is intangible and complex.To study low-frequency oscillations, including local and inter-area oscillations, a system with six machines and two areas was considered as the system under study. Wind farms were properly located in one area of the system. Each area system consists of two machines connected via two 220 km transmission lines. The power, injected by wind systems into the network, was 200 MW. With the different disturbances occurrence in the power system, oscillations with different frequency ranges may appear in the system. In this section, the investigated fault is a three-phase short-circuit fault that occurred in the middle of the line and lasted 200 ms. this fault was followed by various low-frequency oscillations such as inter-area oscillations. In this regard, the main purpose was to dampen these oscillations and maintain the system stability.

Using the SSA optimization algorithm for zero-time delay, the parameters of the WADC, which is added to the reactive power control loop of the DFIG-based wind, were optimally determined.

7. References

[1] X. Shi et al., "Data-driven model-free adaptive damping control with unknown control direction for wind farms," *Int. J. Electr. Power Energy Syst., vol. 123, no. May, 2020.*

[2] M. J. Alinezhad, M. Radmehr, and S. Ranjbar, "Adaptive wide area damping controller for damping inter-area oscillations considering high penetration of wind farms," *Int. Trans. Electr. Energy Syst., vol. 30, no. 6, pp. 1–21, 2020.*

[3] N. Gurung, R. Bhattarai, and S. Kamalasadan, "Optimal Oscillation Damping Controller Design for Large-Scale Wind Integrated Power Grid," *IEEE Trans. Ind. Appl., vol. 56, no. 4, pp. 4225–4235, 2020.*

[4] J. Nan et al., "Wide-area power oscillation damper for DFIG-based wind farm with communication delay and packet dropout compensation," *Int. J. Electr. Power Energy Syst., vol. 124, no. May 2020, p. 106306, 2021.*

[5] L. Khan and K. L. Lo, "Hybrid micro-GA based FLCs

for TCSC and UPFC in a multi-machine environment," *Electr. Power Syst. Res., vol. 76, no. 9–10, pp. 832–843, Jun. 2006.*

[6] G. Rogers, Power system oscillations. *Kluwer Academic Publishers, 2000.*

[7] P. Kundur, N. J. Balu, and M. G. Lauby, *Power system stability and control. McGraw-Hill, 1994.*

[8] A. Feliachi, "Stabilization of inter-area oscillation modes through excitation systems," *IEEE Trans. Power Syst., vol. 9, no. 1, pp. 494–502, 1994.*

[9] E. V. Larsen, J. J. Sanchez-Gasca, and J. H. Chow, "Concepts for design of FACTS controllers to damp power swings," *IEEE Trans. Power Syst., vol. 10, no. 2, pp. 948–956, May 1995.*

[10] W. Yao, L. Jiang, Q. H. Wu, J. Y. Wen, and S. J. Cheng, "Delay-dependent stability analysis of the power system with a wide-area damping controller embedded," *IEEE Trans. Power Syst., vol. 26, no. 1, pp. 233–240, 2011.*

[11] H. Shayeghi, H. A. Shayanfar, A. Safari, and R. Aghmasheh, "A robust PSSs design using PSO in a multi-machine environment," *Energy Convers. Manag., vol. 51, no. 4, pp. 696–702, Apr. 2010.*

[12] J. da Cruz and L. Cera Zanetta, "Stabilizer design for multimachine power systems using mathematical programming," *Int. J. Electr. Power Energy Syst., vol. 19, no. 8, pp. 519–523, 1997.*

[13] L. C. Zanetta and J. J. Da Cruz, "An incremental approach to the coordinated tuning of power systems stabilizers using mathematical programming," *IEEE Trans. Power Syst., vol. 20, no. 2, pp. 895–902, 2005.*

[14] P. Rokni Nakhi and M. Ahmadi Kamarposhti, "Multi objective design of type II fuzzy based power system stabilizer for power system with wind farm turbine considering uncertainty," *Int. Trans. Electr. Energy Syst., 2019.*

[15] A. Bose, "Smart Transmission Grid Applications and Their Supporting Infrastructure," *IEEE Trans. Smart Grid, vol. 1, no. 1, pp. 11–19, Jun. 2010.*

[16] M. Mokhtari, F. Aminifar, D. Nazarpour, and S. Golshannavaz, "Wide-area power oscillation damping with a fuzzy controller compensating the continuous communication delays," *IEEE Trans. Power Syst., vol. 28, no. 2, pp. 1997–2005, 2013.*

[17] B. Naduvathuparambil, M. C. Valenti, and A. Feliachi, "Communication delays in wide area measurement systems," *in Proceedings of the Thirty-Fourth Southeastern Symposium on System Theory (Cat. No.02EX540), 2002, pp. 118–122.*

[18] L. D. Philipp, A. Mahmood, and B. L. Philipp, "An improved refinable rational approximation to the ideal time delay," *IEEE Trans. Circuits Syst. I Fundam. Theory Appl., vol. 46, no. 5, pp. 637–640, May 1999.*

[19] S. Arabi Nowdeh et al., "Fuzzy multi-objective placement of renewable energy sources in distribution system with objective of loss reduction and reliability improvement using a novel hybrid method," *Appl. Soft Comput., vol. 77, pp. 761–779, Apr. 2019.*

[20] M. Jahannoosh, S. A. Nowdeh, A. Naderipour, H. Kamyab, I. F. Davoudkhani, and J. J. Klemeš, "New hybrid meta-heuristic algorithm for reliable and cost-effective designing of photovoltaic/wind/fuel cell energy system considering load interruption probability," *J. Clean. Prod., vol. 278, 2021.*

[21] S. Mirjalili, A. H. Gandomi, S. Z. Mirjalili, S. Saremi, H. Faris, and S. M. Mirjalili, "Salp Swarm Algorithm: A bio-inspired optimizer for engineering design problems," *Adv. Eng. Softw., vol. 114, pp. 163–191, 2017.*

[22] A. Naderipour et al., "Carrier wave optimization for multi-level photovoltaic system to improvement of power quality in industrial environments based on Salp swarm algorithm," *Environ. Technol. Innov., 2020.*

[23] M. Mokhtari and F. Aminifar, "Toward Wide-Area Oscillation Control Through Doubly-Fed Induction Generator Wind Farms," *IEEE Trans. Power Syst., vol. 29, no. 6, pp. 2985–2992, Nov. 2014.*

[24] Sauer Peter W, Pai MA. Power system dynamics and stability. Prentice Hall;1998

[25] Abido MA. Parameter optimization of multimachine power system stabilizers using genetic local search. Int J Electr Power Energy Syst 2001;23:785–94.